Macromolecules

pubs.acs.org/Macromolecules Article

Folded Chain Lamellae of Dynamic Helical Poly(phenylacetylene) in the Hexagonal Columnar Phase

Yan-Fang Zhang, Xu Chen, Xiao-Song Yu, Jia-Xin Chen, Ming-Qiu Hu, Bo-Yuan Zheng, Yi-Xin Liu,* Shuang Yang,* and Er-Qiang Chen*

Cite This: *Macromolecules* 2021, 54, 6038−6044 Read Online

ACCESS | Metrics & More | Article Recommendations | Supporting Information

ABSTRACT: Long-chain molecules can self-assemble into ordered and functional structures through chain folding. In crystalline polymers, chain folding leads to lamellar crystals that are extremely important to the ultimate properties. Understanding chain folding at the molecular level remains a great challenge. Here, we report that a dynamic helical *cis*-poly(phenylacetylene) bearing a bulky side group (**P1**), which is a side-chain liquid crystalline polymer, can also form folded chain lamellae in the hexagonal columnar phase. Our atomic force microscopy (AFM) experiments on **P1** thin films directly visualized the adjacent and nonadjacent folds at the liquid crystal−amorphous interface. While the helical segments of **P1** with a diameter of 2.2 nm closely pack in the hexagonal lattice, the disorder strands that connect the helices could compose the folds. Furthermore, we monitored the lamellar growth from the amorphous state using AFM. We demonstrate experimentally for the first time that the lamellar growth may obey the kinetics of Ostwald ripening. It is also found that with the initial lamellar thickness close to the persistence length of **P1**, the lamellae show simultaneous lateral extension and thickening.

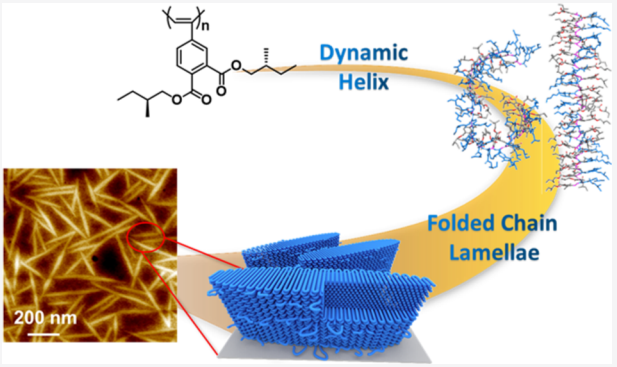

INTRODUCTION

Chain folding is a fundamental mechanism in self-assembly of bio- and nonbiological polymers.[1,2] Proteins fold into their native state of ordered secondary and tertiary structure, based on which biological functions are demonstrated.[1] For synthetic long-chain polymers, folding prevails when a random coil collapses into a globule.[3] Importantly, crystalline polymers invoke chain folding as the elementary step to form lamellar crystals,[2,4−8] which affords the fast pathway of free energy reduction when the metastable liquid turns into crystals. As vital to the definitive utilities of crystalline polymers, which are applied everyway, lamellar crystals have been a formidable subject in both experiment and theory for decades. Nonetheless, the mechanism of chain folding crystallization remains unclear,[9−14] and thus the legible and intact pictures at the molecular level are highly desired.

Albeit enormous difficulties, direct visualization of folded chains has been attained using atomic force microscopy (AFM).[15−17] Torsional-tapping AFM was developed to detect the molecular conformations of polyethylene (PE) chains at the crystal−amorphous interface.[15,16] For the monolayer of *isotactic* poly(methyl methacrylate) (*i*-PMMA) on the mica surface prepared using the Langmuir−Blodgett technique, AFM experiments revealed the chain folding of the double-stranded helix of *i*-PMMA in the monolayer as well as the growth of two-dimensional (2D) crystals.[18,19] Compared with flexible PE chains, the double-stranded helix is much more rigid, and its folding is fascinating. *Cis*-poly(phenylacetylene) (*cis*-PPA) is a typical dynamic helical polymer.[20,21] The chain diameter, helical handedness, helical pitch, and helical reversal have been successfully uncovered under a high-resolution atomic force microscope.[22−27] In the mono- or double layers on the solid substrate, the *cis*-PPA chains are observed to pack parallel into 2D crystals[22−24] or 2D nematic liquid crystals,[28,29] wherein the chains adopt an *extended* conformation as expected for the rigid polymers. It is interesting to ask whether the dynamic helical character of *cis*-PPA chains can permit chain folding, and furthermore, how the chains will organize into a hierarchical structure and morphology with the ordering on different length scales.

Herein, we report that a *cis*-PPA, which bears two chiral (*S*)-2-methylbutyl moieties attached to the 3,4-position of the phenyl group through ester linkages (**P1**, Chart 1), can

Received: April 14, 2021
Revised: May 29, 2021
Published: June 16, 2021

https://doi.org/10.1021/acs.macromol.1c00818
Macromolecules 2021, 54, 6038−6044

Chart 1. Chemical Structure of P1.

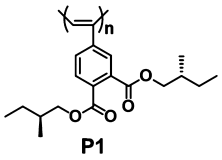

implement chain folding in the thin film. The film thickness of 50 nm is nearly twice the radius of gyration (R_g) of the polymer studied. Particularly, the chain folding of **P1** occurs in a hexagonal columnar liquid crystal phase (Col_H) rather than in a crystal phase, which could proceed to edge-on lamellae on the solid substrate. We followed the growth of folded chain lamellae of **P1**. Tapered lamellae are observed with simultaneous lateral growth and thickening, like that found in PE lamellae in the hexagonal phase.[30,31] However, the **P1** lamellar growth exhibits the kinetics of Ostwald ripening,[32,33] in contrast to the expected nucleation- or diffusion-controlled growth. To the best of our knowledge, this is the first experimental result of Ostwald ripening reported for the growth of folded chain lamellae.

RESULTS AND DISCUSSION

Synthesis and molecular characterization of **P1** are detailed in the Supporting Information. It was found that the dynamic helical **P1** chains with a *cis*-content of 90% could be well dissolved in common organic solvents such as chloroform, tetrahydrofuran, cyclohexane, *etc.* Solution light scattering indicates that **P1** has a weight-average molecular weight of 1.41 × 10^6 g mol^{-1} and a R_g of ~34 nm (Figure S1). Assuming 0.22 nm as the monomer unit length,[34] the persistence length (l_p) of **P1** was estimated to be ~6 nm. It is worth noting that although the alkyl tail on the side group of **P1** bears the chiral center, circular dichroism (CD) of both the **P1** solution and solid film is null in signal (Figure S2). Presumably, this could be due to that the chiral center situated at the second carbon of the alkyl tail is a little far away from the PPA backbone so that the chirality could not be effectively transferred to induce the single-handed helix with a preferential handedness. The CD result suggests that **P1** shall possess the right- and left-handed helical segments coexisting along the chain, which are connected by the disordered strands.

P1 with the bulky pendants presents the thermodynamically stable phase of Col_H, similar to the extensively studied helical dendronized or side-chain PPAs.[35−40] Nonetheless, precipitation and solution casting could result in amorphous **P1** (Figure 1a, black line). At or above 100 °C, when the conformation isomerization between *cis*-cisoidal (*c*-c) and *cis*-transoidal (*c*-t) becomes active,[35,36,40] thermal annealing turned the amorphous **P1** into Col_H. The annealing temperature (T_a) applied in the experiments did not exceed 120 °C because at higher T_a the intramolecular cyclization and chain scission of **P1** would become severe when the annealing time was prolonged.[41] Due to the same reason, the isotropic temperature of Col_H, which should be higher than the decomposition temperature, could not be certainly determined upon heating.

The Col_H of **P1**, wherein the parallel molecular cylinders are closely packed, is confirmed by X-ray diffraction (XRD) of the well-annealed samples (blue line in Figure 1a). While an amorphous halo is observed in the high-angle region, a set of low-angle diffractions with a *q*-ratio ($q = 4\pi\sin\theta/\lambda$, with 2θ the

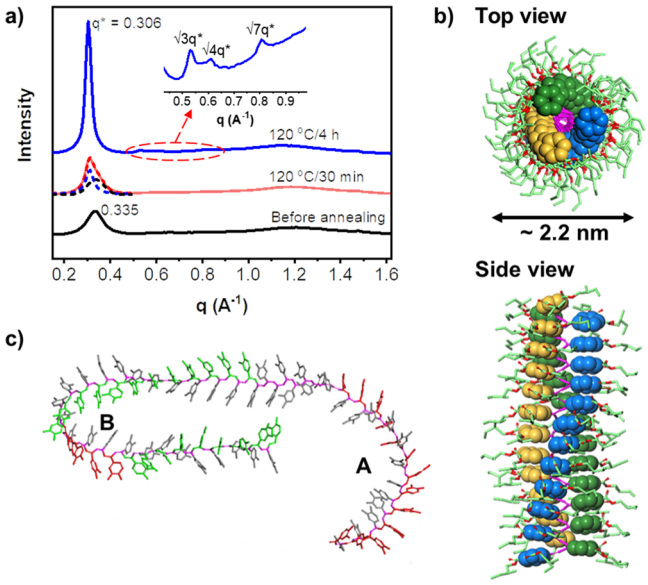

Figure 1. (a) 1D XRD profiles of **P1** recorded at room temperature (RT). The original sample was obtained by solution casting at RT. The black, red, and blue solid lines correspond to the sample before annealing, annealing for 0.5, and 4 h at 120 °C, respectively. The major low-angle peak in the red line is in fact composed of the Col_H diffraction and the amorphous scattering, which can be deconvoluted as represented by dotted blue and black lines, respectively. (b) Molecular modeling of the **P1** helix with a dihedral angle of 70°, i.e., suitable in the Col_H phase. (c) Fold conformation of the **P1** strand obtained by molecular simulations. The dihedral angles are around 140°. The phenylene groups with green and red colors indicate the left- and right-handed helical segments, respectively. Chain folding can be achieved by continuous bending (A) and helical reversal (B).

scattering angle and λ the X-ray wavelength) of $1:3^{1/2}:4^{1/2}:7^{1/2}$ indicates a hexagonal lattice with a parameter *a* of 2.22 nm. Molecular simulation suggests that in Col_H, the **P1** helix adopts a *c*-c conformation with a dihedral angle of 70° (Figure 1b), of which the diameter of 2.2 nm matches the *a* parameter. Such a **P1** helix has the lowest energy among the *c*-c conformations with various dihedral angles (Figure S4).

We performed AFM at RT to investigate the structure and morphology of **P1** in the 50 nm-thick thin film on the silicon substrate, which was spin cast from the cyclohexane dilute solution. Fascinatingly, we found that after thermal annealing, the film surface would be covered by lath-like entities or lamellae (Figures 2a and S5). Grazing-incidence XRD indicates that the Col_H phase is well developed in the thin film (Figure 2b). The strong out-of-plane (10) diffraction of the hexagonal lattice evidences that the **P1** segments are parallel to the substrate. In this case, the lath-like entities can be viewed as edge-on lamellae, as schematically drawn in the inset of Figure 2b. In polymer thin film crystallization, edge-on lamellae can be frequently observed.[42]

When zooming in the scanning area (Figures 2c−f, S6), we verified that the **P1** lamellae are composed of the **P1** chain segments or stems parallelly packed together. The mean width of stems in the lamellae is 2.2 nm, consistent with the XRD results. Careful examination of **P1** lamellae can further unveil many important issues that have been intensively discussed in polymer crystallization.[2,4−14] The blue lines in Figure 2d,f are drawn to illustrate the possible conformations of **P1** chains observed in the enlarged AFM images of Figure 2d,f. Clearly,

https://doi.org/10.1021/acs.macromol.1c00818
Macromolecules 2021, 54, 6038−6044

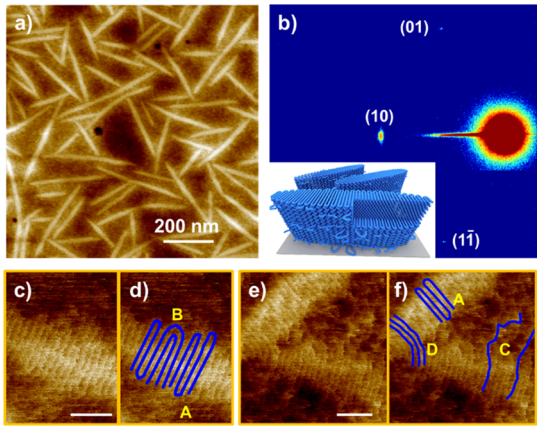

Figure 2. (a) AFM height image and (b) grazing-incidence XRD pattern of **P1** thin films after annealing at 120 °C for 2 h. The inset in (b) shows the schematic of edge-on lamellae. (c,e) Zoomed AFM images. (d,f) Schematic representation of possible chain conformations shown in (c,e). A, B, C, and D indicate the adjacent, nonadjacent folded chain, dangling cilia emanating from the lamellar folded surface, and tie chains that join two lamellae, respectively. Scale bar: 10 nm.

there exist adjacent and nonadjacent chain foldings, dangling cilia emanating from the lamellar folded surface, and tie chains that join two lamellae. Moreover, the stems within a lamella exhibit a length distribution, giving direct evidence of the fold length fluctuation.

A perfect **P1** helix with a dihedral angle of 70° is a rigid rod (Figures 1b and S4) that is hard to bend. The chain folding observed must be associated with some "wrong" conformations existing in the **P1** chain. Note that a value of ~6 nm of l_p for **P1** is remarkably smaller than that reported for other PPAs,[34] suggesting that the chain is just semirigid. Figure 1c shows a possible fold conformation of a **P1** strand simulated, wherein the dihedral angles are around 140° (Figure S4). In this case, the pendants are more apart from each other, releasing partly the steric hindrance. The chain thus becomes relatively flexible and can continuously bend into a fold (A in Figure 1c). Moreover, the fold can also consist of the helical reversal (B in Figure 1c). Such disordered strands might not regulate conformation timely during the development of Col_H. We conjecture that because they cannot closely pack together, the segments with "wrong" conformations will be rejected by Col_H and be cumulated on the lamellar basal surface. Meanwhile, chain folding helps **P1** chains to avoid surface overcrowding when they assemble into lamellae, the same as that occurred in crystallization of polymers.[6] Likely, the "wrong" segments can further act as "impurities" to cause the lamellar branching and separating.[2,4] Figure 2a shows that the individual lamellae orientate randomly, and there exist no sheaf-like stacks of lamellae, which are usually found in polymer crystals.[2,4] As shown by D in Figure 2f, even two lamellae that are tied by some common **P1** segments are splayed apart.

To monitor the lamellar growth of **P1**, we tried in situ AFM at above 100 °C but failed because of the severe thermal drift. Fortunately, we found that the Col_H evolution could be interrupted when shifting the temperature from T_a to RT. As depicted by the red line in Figure 1a, the XRD result indicates that the sample quenched to RT after a short annealing at 120 °C consisted of the Col_H and amorphous **P1**. Prolonged staying at RT would not increase the liquid crystallinity. This allows us to conduct quasi-in situ AFM. Namely, after annealing at a fixed T_a for a period of t, the sample was quenched to RT for AFM scan; subsequently, the sample was brought back to T_a quickly to resume the lamellar growth for an additional t. Repeating this procedure could catch the morphology change with t in the same area. Figure 3 shows a set of quasi-in situ AFM images of a **P1** thin film annealed at T_a = 110 °C. After 30 min, the lamellae can be clearly sensed. As the amorphous **P1** at 110 °C is a viscous fluid, the lamellae may slightly change their orientation during growth. Nonetheless, the same lamellae can be identified visibly in the sequential AFM images, as exemplified by lamellae A, B, C, and D in Figure 3.

Different modes of lamella growth could be identified based on the quasi-in situ AFM results. The lamella may grow freely

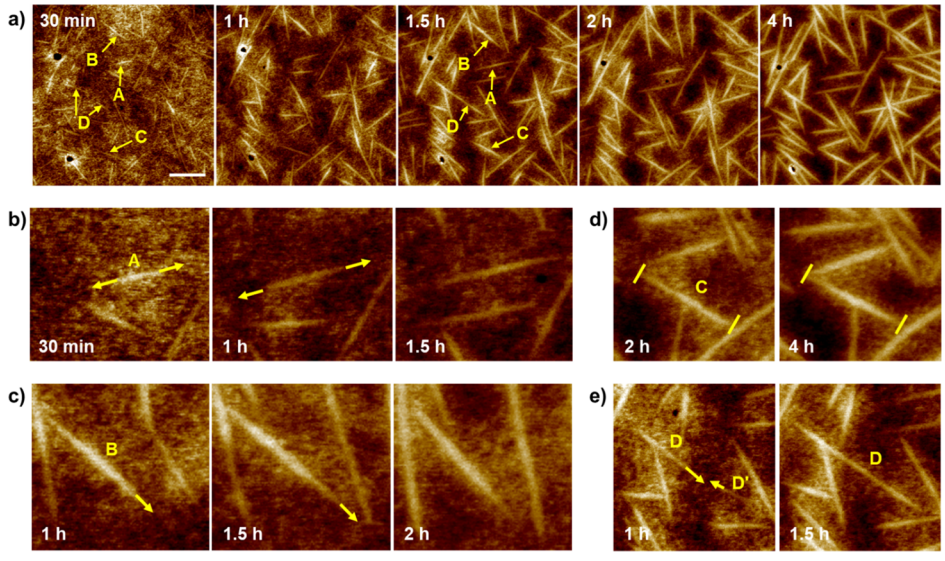

Figure 3. (a) Quasi-in situ AFM height images of the **P1** thin film annealed at 110 °C for different times. Scale bar: 200 nm. (b–e) Zoomed AFM images representing different growth modes of lamellae A–D indexed in (a). (b) Lamella A: free growth toward both sides. (c) Lamella B: one side growth. (d) Lamella C: cease of growth on both sides. (e) Lamella D: merging of two separated lamellae into one.

https://doi.org/10.1021/acs.macromol.1c00818
Macromolecules 2021, 54, 6038–6044

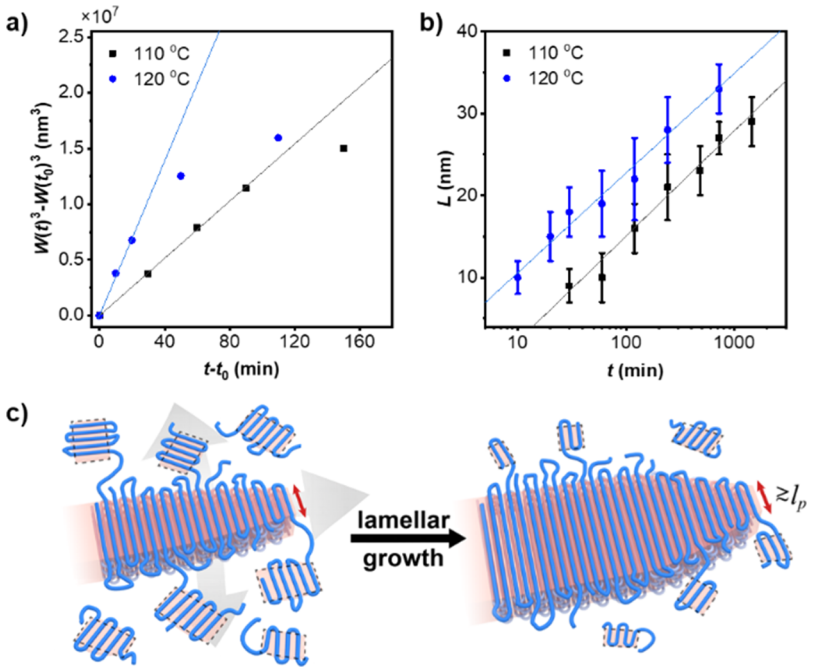

Figure 4. (a) Plots of $W(t)^3 - W(t_0)^3$ vs $t - t_0$ for T_as of 110 and 120 °C. $W(t)$ is the mean length of the freely growing lamellae at annealing time t. (b) Lamellar thickness L as a function of log t. L is the lamellar thickness at the lamellar center portion measured by ex situ AFM. (c) Schematic of growth of folded chain lamella of **P1**. The dashed rectangles indicate the clusters of helical segments in the amorphous regions. Dissolution of the clusters provides the materials for the lamellar growth, resulting in the kinetics of Ostwald ripening. The lamellar growth tip has a width close to l_p of **P1**. Lateral growth and lamellar thickening occur simultaneously, resulting in the tapered morphology.

toward both sides (Figure 3b), or only one side is extended when the other side encounters another lamella (Figure 3c). When both sides are blocked by other lamellae, the lamella ceases in the lateral growth (Figure 3d). When two separated lamellae grow nearly head to head, they may merge into one (Figure 3e). Seemingly, the **P1** chains between the two growth tips shown in Figure 3e could join in both lamellae simultaneously and thus weld them together. For T_a = 120 °C, the same lamellar growth behavior can be observed (Figure S8).

We measured the lengths of individual lamellae that changed with t (Figure S9 and 10). Attention was paid to the lamellae growing freely toward both sides, of which the mean lamellar length (W) was calculated (see Supporting Information for the details). The overall trend of morphology evolution could be well represented by W as a function of t (Figures S9 and 10). Two stages can be recognized: W increases *nonlinearly* first and then, as the lamellar growth tips approach other lamellae nearby, W tends to level off. Interestingly, we find that for the first stage, W is proportional to $t^{1/3}$, evidenced by the linear line passing through the origin in the plot of $W(t)3 - W(t_0)3$ versus $t - t_0$,[32] wherein t_0 is the time for the first observation of lamellae under an atomic force microscope (Figure 4a). Consequently, the nucleation- and diffusion-controlled growth of **P1** lamellae, which shall correspond to W proportional to t and $t^{1/2}$, respectively, could be excluded.

The scaling of $W \sim t^{1/3}$ suggests that the lamellar growth of **P1** follows the mechanism of Ostwald ripening.[32,33] A conventional Ostwald ripening would normally be observed in the late stage of a diffusion-controlled growth process. In a collection of particles with a size distribution, large particles will grow in the expense of materials from the small particles. Here, the small particles are less stable than the larger particles because the former has higher surface energy. In our case, as mentioned, the long **P1** chain consists of helical segments and disorder segments linked together. After the solvent was eliminated, in the spin cast film, the **P1** chains collapse, and the helical segments could condense together to form clusters pervasively.[11,12,14,43] When the motion of **P1** chains becomes active at high temperatures, part of the clusters evolve into nuclei and further the lamellae. The lamellar growth needs to consume the chain segments with correct conformation, that is, the helical segments, thus largely relying on the dissolution of other less-stable clusters, as suggested by the schematic in Figure 4c. This process can be analogized to the "evaporation−condensation" occurring in the conventional Ostwald ripening, by noticing that the growing lamellae and the diminishing clusters of helical segments can be viewed as the large growing particles and the evaporating particles, respectively. Note that the clusters of helical segments cannot directly be detected by our AFM due to the limit of resolution, thus only the averaging length of the lamellae W is reported in Figure 4. The size of these selected lamellae should be well above the actual averaging size of all particles, which include the less-stable clusters and lamellar nuclei. Nonetheless, the characteristic scaling of the Ostwald ripening should still preserve (see Data Analysis of Ostwald Ripening in Supporting Information).

Worthy of note is the high number density of lamellae that grow independently at the same time (~80 and ~90 per μm2 for 110 and 120 °C, respectively). Thus, in the late stage of the growth process, these growing lamellae compete fiercely in the consumption of the helical segments, leading to the shortage of the less-stable clusters of helical segments. Consequently, the Ostwald ripening is no longer sustainable and the W versus t curve deviates from the $t^{1/3}$ scaling law accordingly. Figure 4a shows that the slope of $W(t)^3 - W(t_0)^3$ versus $t - t_0$ is larger for 120 °C than that for 110 °C, indicating the accelerated lamellar growth at an elevated temperature, which should be

https://doi.org/10.1021/acs.macromol.1c00818
Macromolecules 2021, 54, 6038−6044

associated with the higher chain mobility. In this sense, the **P1** lamellar growth in the Col_H phase from the amorphous state could be reminiscent of polymer cold crystallization, which takes place by bringing the polymer from the amorphous state of glass to above the glass transition temperature.

From the sequential AFM images shown in Figure 3a, one may be already aware of that the **P1** lamellae become thicker and thicker during annealing. Moreover, the lamellae are tapered from the center to the growth tip. The tapered shape looks like that of PE lamellae grown in the hexagonal phase, suggesting that the lateral growth and lamellar thickening occur simultaneously.[30,31] The thickening may be achieved either by longitudinal sliding diffusion or by conformation adjustment of **P1** segments in the fold loops and cilia on the lamellar basal surface. To measure the lamellar thickness (L) more precisely, we used ex situ AFM images with higher resolution (Figure S11 and 12). Figure 4b plots the L measured at the lamellar center portion against the logarithm of annealing time (log t), wherein fairly a linear function can be recognized. In this case, the lamellar thickening of **P1** differs from that of PE in the hexagonal phase, where L increases linearly with t,[30,31] but rather like that of PE occurred in the orthorhombic phase.[44,45] The extended chain lamella of **P1** cannot be attained, probably due to that some "wrong" conformations are unable to be adjusted thoroughly and the existence of chain entanglement. It is interesting to note that the spontaneously occurring lateral growth of lamellae and lamellar thickening present distinct and independent kinetics, that is, $W \sim t^{1/3}$ and $L \sim \log t$, respectively. This may reflect that the diffusion process of Ostwald ripening mainly occurs at the two growing tips of each lamella. On the other hand, the lamellar thickening is a local process associated with the folds and cilia on the lamellar basal surfaces.

Similar to that occurred in polymer crystallization,[2,4−14] the higher the T_a, the thicker the lamellae of **P1**. For t = 240 min, the mean values of L at the lamellar center are 21 and 28 nm for 110 and 120 °C, respectively; however, at the early stage, the difference between the L values at these two T_as is just ∼1 nm (Figure 4b). This outcome indicates that the thickening process in fact dominates how large the L can be reached.[13] On the other hand, when measuring the lamellar tip widths at various ts, we find that they are roughly constant, which are ∼8 and ∼9 nm at 110 and 120 °C, respectively (Figures 5 and S13). For crystalline polymer, the metastable lamellae always tend to thicken to reduce the free energy, and thus the initial lamellar thickness is somewhat hard to be ambiguously determined. Here, the tip width may reflect the initial lamellar thickness of **P1**. Intriguingly, we note that this size is just slightly larger than the l_p value of ∼6 nm for **P1**. We envisage that because the **P1** chains intend to assemble into Col_H as quickly as possible, the existing helical segments with l_p will be selected at first.[11,12] With no need of too much conformation regulation, they can fit into the lattice on the lamellar growth front.

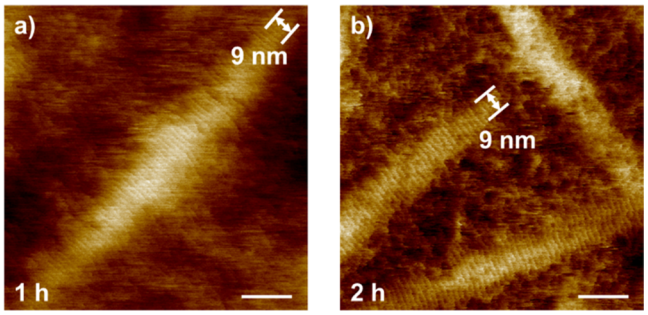

Figure 5. Ex situ AFM height images of **P1** thin films annealed at 120 °C for different times. (a,b), t = 1 and 2 h, respectively. Scale bar: 20 nm. The double-sided arrows indicate the width of lamellar growth tips.

CONCLUSIONS

In summary, we demonstrate that **P1**, a dynamic helical poly(phenylacetylene), can form folded chain lamellae in its Col_H phase. Direct visualization of **P1** chains under an atomic force microscope reveals many important issues of chain folding as extensively studied in polymer crystallization, corroborating chain folding as an essential mechanism in the self-assembly of polymers toward the ordered hierarchical structures. Our ongoing experiments indicate that, similar to **P1**, other PPAs with alkyl tails attached to the 3,4- or 3,5-position of the phenyl group via ester linkage could also form folded chain lamellae. We suggest that while the helical segments pack into the Col_H lamellae, the disordered strands compose the folds. The lamellae of **P1** exhibit a coupled lateral growth and lamellar thickening, with the initial lamellar thickness tightly associated with the persistence length of the polymer. It is also identified that the lamellar growth follows the kinetics of Ostwald ripening. This may be due to the semirigid **P1** forms numerous dense clusters of helical segments as precursors to the Col_H phase. When many lamellae compete with each other, the clusters that hamper the chain diffusion would make a shortage of materials available for lamellar growth. We presume that this case may also occur in the cold crystallization of conventional semicrystalline polymers. We hope this work will inspire more research studies on polymer self-assembly involving chain folding.

ASSOCIATED CONTENT

Supporting Information

The Supporting Information is available free of charge at https://pubs.acs.org/doi/10.1021/acs.macromol.1c00818.

Experiments and data analysis; solution light scattering results; CD spectra; 2D XRD pattern and reconstructed electron density map; molecular mechanics simulation results; GI-XRD pattern; quasi-in situ and ex situ AFM height images; and synthesis and molecular characterization (PDF)

AUTHOR INFORMATION

Corresponding Authors

Yi-Xin Liu − *State Key Laboratory of Molecular Engineering of Polymers, Department of Macromolecular Science, Fudan University, Shanghai 200438, China;* orcid.org/0000-0001-9374-5981; Email: lyx@fudan.edu.cn

Shuang Yang − *Beijing National Laboratory for Molecular Sciences, Key Laboratory of Polymer Chemistry and Physics of Ministry of Education, Center for Soft Matter Science and Engineering, College of Chemistry, Peking University, Beijing 100871, China;* orcid.org/0000-0002-5573-5632; Email: shuangyang@pku.edu.cn

Er-Qiang Chen − *Beijing National Laboratory for Molecular Sciences, Key Laboratory of Polymer Chemistry and Physics of Ministry of Education, Center for Soft Matter Science and*

https://doi.org/10.1021/acs.macromol.1c00818
Macromolecules 2021, 54, 6038−6044

Engineering, College of Chemistry, Peking University, Beijing 100871, China; orcid.org/0000-0002-0408-5326; Email: eqchen@pku.edu.cn

Authors

Yan-Fang Zhang − *Beijing National Laboratory for Molecular Sciences, Key Laboratory of Polymer Chemistry and Physics of Ministry of Education, Center for Soft Matter Science and Engineering, College of Chemistry, Peking University, Beijing 100871, China*

Xu Chen − *Beijing National Laboratory for Molecular Sciences, Key Laboratory of Polymer Chemistry and Physics of Ministry of Education, Center for Soft Matter Science and Engineering, College of Chemistry, Peking University, Beijing 100871, China*

Xiao-Song Yu − *Beijing National Laboratory for Molecular Sciences, Key Laboratory of Polymer Chemistry and Physics of Ministry of Education, Center for Soft Matter Science and Engineering, College of Chemistry, Peking University, Beijing 100871, China*

Jia-Xin Chen − *Beijing National Laboratory for Molecular Sciences, Key Laboratory of Polymer Chemistry and Physics of Ministry of Education, Center for Soft Matter Science and Engineering, College of Chemistry, Peking University, Beijing 100871, China*

Ming-Qiu Hu − *Beijing National Laboratory for Molecular Sciences, Key Laboratory of Polymer Chemistry and Physics of Ministry of Education, Center for Soft Matter Science and Engineering, College of Chemistry, Peking University, Beijing 100871, China*

Bo-Yuan Zheng − *Beijing National Laboratory for Molecular Sciences, Key Laboratory of Polymer Chemistry and Physics of Ministry of Education, Center for Soft Matter Science and Engineering, College of Chemistry, Peking University, Beijing 100871, China*

Complete contact information is available at: https://pubs.acs.org/10.1021/acs.macromol.1c00818

Funding

This work was supported by the National Natural Science Foundation of China (51921002, 216340010, and 21873021) and the National Key R&D Program of China (2018YFB0703703).

Notes

The authors declare no competing financial interest.

■ ACKNOWLEDGMENTS

We are grateful to Profs. T. Miyoshi and D. H. Liang for their help in molecular characterization.

■ REFERENCES

(1) Whitford, D. *Proteins: Structure and Function*; John Wiley & Sons Ltd: West Susses, 2005.
(2) Wunderlich, B. *Macromolecular Physics*, 1st ed.; Academic Press: New York, 1976; Vol. *1*.
(3) Wu, C. *Macromolecular Solutions*; Higher Education Press: Beijing, 2021.
(4) Bassett, D. C. *Principles of Polymer Morphology*, 1st ed.; Cambridge University Press: England, 1981; p 259.
(5) Armitstead, K.; Goldbeck-Wood, G.; Keller, A. Polymer Crystallization Theories. *Macromolecules: Synthesis, Order and Advanced Properties*; Advances in Polymer Science; Springer, 1992;Vol. *100*, pp 221−312.
(6) Hoffman, J. D.; Miller, R. L. Kinetic of Crystallization from the Melt and Chain Folding in Polyethylene Fractions Revisited: Theory and Experiment. *Polymer* **1997**, *38*, 3151−3212.
(7) Cheng, S. Z. D. *Phase Transitions in Polymers: The Role of Metastable States*, 1st ed.; Elsevier: Amsterdam, 2008; p 324.
(8) Lotz, B.; Miyoshi, T.; Cheng, S. Z. D. 50th Anniversary Perspective: Polymer Crystals and Crystallization: Personal Journeys in a Challenging Research Field. *Macromolecules* **2017**, *50*, 5995−6025.
(9) Strobl, G. *The Physics of Polymers*, 3rd ed.; Springer: New York, 2007.
(10) Muthukumar, M. Commentary on Theories of Polymer Crystallization. *Eur. Phys. J. E* **2000**, *3*, 199−202.
(11) Allegra, G.; Meille, S. V. Pre-Crystalline, High-Entropy Aggregates: A Role in Polymer Crystallization?. *Interphases and Mesophases in Polymer Crystallization III*; Advances in Polymer Science; Springer, 2005; Vol. *191*, pp 87−135.
(12) Subirana, J. A. Elucidation of Chain Folding in Polymer Crystals: Comparison with Proteins. *Trends Polym. Sci.* **1997**, *5*, 321−326.
(13) Welch, P.; Muthukumar, M. Molecular Mechanisms of Polymer Crystallization from Solution. *Phys. Rev. Lett.* **2001**, *87*, 218302.
(14) Tang, X.; Chen, W.; Li, L. The Tough Journey of Polymer Crystallization: Battling with Chain Flexibility and Connectivity. *Macromolecules* **2019**, *52*, 3575−3591.
(15) Mullin, N.; Hobbs, J. K. Direct Imaging of Polyethylene Films at Single-Chain Resolution with Torsional Tapping Atomic Force Microscopy. *Phys. Rev. Lett.* **2011**, *107*, 197801.
(16) Savage, R. C.; Mullin, N.; Hobbs, J. K. Molecular Conformation at the Crystal-Amorphous Interface in Polyethylene. *Macromolecules* **2015**, *48*, 6160−6165.
(17) Kumaki, J. Observation of Polymer Chain Structures in Two-Dimensional Films by Atomic Force Microscopy. *Polym. J.* **2016**, *48*, 3−14.
(18) Kumaki, J.; Kawauchi, T.; Yashima, E. Two-Dimensional Folded Chain Crystals of a Synthetic Polymer in a Langmuir−Blodgett Film. *J. Am. Chem. Soc.* **2005**, *127*, 5788−5789.
(19) Ono, Y.; Kumaki, J. In Situ Real-Time Observation of Polymer Folded-Chain Crystallization by Atomic Force Microscopy at the Molecular Level. *Macromolecules* **2018**, *51*, 7629−7636.
(20) Freire, F.; Quiñoá, E.; Riguera, R. Supramolecular Assemblies from Poly(phenylacetylene)s. *Chem. Rev.* **2016**, *116*, 1242−1271.
(21) Yoshida, Y.; Mawatari, Y.; Motoshige, A.; Motoshige, R.; Hiraoki, T.; Wagner, M.; Müllen, K.; Tabata, M. Accordion-like Oscillation of Contracted and Stretched Helices of Polyacetylenes Synchronized with the Restricted Rotation of Side Chains. *J. Am. Chem. Soc.* **2013**, *135*, 4110−4116.
(22) Sakurai, S.-i.; Okoshi, K.; Kumaki, J.; Yashima, E. Two-Dimensional Hierarchical Self-Assembly of One-Handed Helical Polymers on Graphite. *Angew. Chem., Int. Ed.* **2006**, *45*, 1245−1248.
(23) Sakurai, S.-i.; Okoshi, K.; Kumaki, J.; Yashima, E. Two-Dimensional Surface Chirality Control by Solvent-Induced Helicity Inversion of a Helical Polyacetylene on Graphite. *J. Am. Chem. Soc.* **2006**, *128*, 5650−5651.
(24) Sakurai, S.-i.; Ohsawa, S.; Nagai, K.; Okoshi, K.; Kumaki, J.; Yashima, E. Two-Dimensional Helix-Bundle Formation of a Dynamic Helical Poly(Phenylacetylene) with Achiral Pendant Groups on Graphite. *Angew. Chem., Int. Ed.* **2007**, *46*, 7605−7608.
(25) Louzao, I.; Seco, J. M.; Quiñoá, E.; Riguera, R. Control of the Helicity of Poly(Phenylacetylene)s: from the Conformation of the Pendant to the Chirality of the Backbone. *Angew. Chem., Int. Ed.* **2010**, *49*, 1430−1433.
(26) Freire, F.; Seco, J. M.; Quiñoá, E.; Riguera, R. Chiral Amplification and Helical-Sense Tuning by Mono- And Divalent Metals on Dynamic Helical Polymers. *Angew. Chem., Int. Ed.* **2011**, *50*, 11692−11696.
(27) Ohsawa, S.; Sakurai, S.-i.; Nagai, K.; Banno, M.; Maeda, K.; Kumaki, J.; Yashima, E. Hierarchical Amplification of Macromolecular Helicity of Dynamic Helical Poly(phenylacetylene)s Composed of

Chiral and Achiral Phenylacetylenes in Dilute Solution, Liquid Crystal, and Two-Dimensional Crystal. *J. Am. Chem. Soc.* **2011**, *133*, 108−114.
(28) Percec, V.; Rudick, J. G.; Peterca, M.; Staley, S. R.; Wagner, M.; Obata, M.; Mitchell, C. M.; Cho, W.-D.; Balagurusamy, V. S. K.; Lowe, J. N.; Glodde, M.; Weichold, O.; Chung, K. J.; Ghionni, N.; Magonov, S. N.; Heiney, P. A. Synthesis, Structural Analysis, and Visualization of a Library of Dendronized Polyphenylacetylenes. *Chem.—Eur. J.* **2006**, *12*, 5731−5746.
(29) Percec, V.; Rudick, J. G.; Wagner, M.; Obata, M.; Mitchell, C. M.; Cho, W.-D.; Magonov, S. N. AFM Visualization of Individual and Periodic Assemblies of a Helical Dendronized Polyphenylacetylene on Graphite. *Macromolecules* **2006**, *39*, 7342−7351.
(30) Hikosaka, M.; Rastogi, S.; Keller, A.; Kawabata, H. Investigations on the Crystallization of Polyethylene Under High Pressure: Role of Mobile Phases, Lamellar Thickening Growth, Phase Transformations, and Morphology. *J. Macromol. Sci., Part B: Phys.* **1992**, *31*, 87−131.
(31) Hikosaka, M.; Amano, K.; Rastogi, S.; Keller, A. Lamellar Thickening Growth of an Extended Chain Single Crystal of Polyethylene. 1. Pointers to a New Crystallization Mechanism of Polymers. *Macromolecules* **1997**, *30*, 2067−2074.
(32) Baldan, A. Progress in Ostwald Ripening Theories and Their Applications to Nickel-Base Superalloys, Part I: Ostwald Ripening Theories. *J. Mater. Sci.* **2002**, *37*, 2171−2202.
(33) Tang, Q.; Müller, M.; Li, C. Y.; Hu, W. Anomalous Ostwald Ripening Enables 2D Polymer Crystals via Fast Evaporation. *Phys. Rev. Lett.* **2019**, *123*, 207801.
(34) Okoshi, K.; Sakurai, S.-i.; Ohsawa, S.; Kumaki, J.; Yashima, E. Control of Main-Chain Stiffness of a Helical Poly(Phenylacetylene) by Switching On and Off The Intramolecular Hydrogen Bonding Through Macromolecular Helicity Inversion. *Angew. Chem., Int. Ed.* **2006**, *45*, 8173−8176.
(35) Percec, V.; Rudick, J. G.; Peterca, M.; Wagner, M.; Obata, M.; Mitchell, C. M.; Cho, W.-D.; Balagurusamy, V. S. K.; Heiney, P. A. Thermoreversible Cis−Cisoidal to Cis−Transoidal Isomerization of Helical Dendronized Polyphenylacetylenes. *J. Am. Chem. Soc.* **2005**, *127*, 15257−15264.
(36) Percec, V.; Rudick, J. G.; Peterca, M.; Heiney, P. A. Nanomechanical Function from Self-Organizable Dendronized Helical Polyphenylacetylenes. *J. Am. Chem. Soc.* **2008**, *130*, 7503−7508.
(37) Rosen, B. M.; Wilson, C. J.; Wilson, D. A.; Peterca, M.; Imam, M. R.; Percec, V. Dendron-Mediated Self-Assembly, Disassembly, and Self-Organization of Complex Systems. *Chem. Rev.* **2009**, *109*, 6275−6540.
(38) Liu, X.-Q.; Wang, J.; Yang, S.; Chen, E.-Q. Self-Organized Columnar Phase of Side-Chain Liquid Crystalline Polymers: To Precisely Control the Number of Chains Bundled in a Supramolecular Column. *ACS Macro Lett.* **2014**, *3*, 834−838.
(39) Liu, X.; Wang, J.; Yang, S.; Men, Y.; Sun, P.; Chen, E.-Q. Entropy Effect of Alkyl Tails on Phase Behaviors of Side-Chain-Jacketed Polyacetylenes: Columnar Phase and Isotropic Phase Reentry. *Polymer* **2016**, *87*, 260−267.
(40) Wang, J.; Liu, X.-Q.; Ren, X.-K.; Zhang, B.; Yang, S.; Cao, Y.; Liu, F.; Lotz, B.; Chen, E.-Q. Helical Polyacetylene-Based Switchable Chiral Columnar Phases: Frustrated Chain Packing and Two-Way Shape Actuator. *Chem.—Asian J.* **2016**, *11*, 2387−2391.
(41) Percec, V.; Rudick, J. G.; Aqad, E. Diminished Helical Character in Para-Substituted Cis-Transoidal Polyphenylacetylenes Due to Intramolecular Cyclization. *Macromolecules* **2005**, *38*, 7205−7206.
(42) Liu, Y.-X.; Chen, E.-Q. Polymer Crystallization of Ultrathin Films on Solid Substrates. *Coord. Chem. Rev.* **2010**, *254*, 1011−1037.
(43) Hong, Y.-l.; Yuan, S.; Li, Z.; Ke, Y.; Nozaki, K.; Miyoshi, T. Three-Dimensional Conformation of Folded Polymers in Single Crystals. *Phys. Rev. Lett.* **2015**, *115*, 168301.
(44) Fischer, E. W.; Schmidt, G. F. Long Periods in Drawn Polyethylene. *Angew. Chem., Int. Ed.* **1962**, *1*, 488−499.
(45) Peterlin, A. Crystallization and Annealing of Polyethylene. *Macromol. Chem.* **1964**, *74*, 107−128.

https://doi.org/10.1021/acs.macromol.1c00818
Macromolecules 2021, 54, 6038−6044